© 2019. Published by The Company of Biologists Ltd | Journal of Cell Science (2019) 132, jcs222430. doi:10.1242/jcs.222430

RESEARCH ARTICLE

Exocyst subunit Sec6 is positioned by microtubule overlaps in the moss phragmoplast prior to cell plate membrane arrival

Han Tang[1], Jeroen de Keijzer[1,*], Elysa J. R. Overdijk[1,2], Els Sweep[1,‡], Maikel Steentjes[1,§], Joop E. M. Vermeer[1,3], Marcel E. Janson[1,¶] and Tijs Ketelaar[1,¶]

ABSTRACT

During plant cytokinesis a radially expanding membrane-enclosed cell plate is formed from fusing vesicles that compartmentalizes the cell in two. How fusion is spatially restricted to the site of cell plate formation is unknown. Aggregation of cell-plate membrane starts near regions of microtubule overlap within the bipolar phragmoplast apparatus of the moss *Physcomitrella patens*. Since vesicle fusion generally requires coordination of vesicle tethering and subsequent fusion activity, we analyzed the subcellular localization of several subunits of the exocyst, a tethering complex active during plant cytokinesis. We found that the exocyst complex subunit Sec6 but not the Sec3 or Sec5 subunits localized to microtubule overlap regions in advance of cell plate construction in moss. Moreover, Sec6 exhibited a conserved physical interaction with an ortholog of the Sec1/Munc18 protein KEULE, an important regulator for cell-plate membrane vesicle fusion in *Arabidopsis*. Recruitment of the *P. patens* protein KEULE and vesicles to the early cell plate was delayed upon *Sec6* gene silencing. Our findings, thus, suggest that vesicle-vesicle fusion is, in part, enabled by a pool of exocyst subunits at microtubule overlaps, which is recruited independently of vesicle delivery.

KEY WORDS: Exocyst, Microtubule, Phragmoplast, *Physcomitrella patens*, Cell plate, MAP65

INTRODUCTION

The physical separation of two daughter cells formed during plant cell division occurs through a transient, disk-shaped membrane compartment that expands radially towards the parental cell wall. This membrane compartment is termed the cell plate and its construction culminates in a new cell wall segment dividing two individual plasma membranes (Drakakaki, 2015; Müller and Jürgens, 2015; Smertenko et al., 2017). Cell plate initiation and radial expansion rely on the fusion of vesicles that are supplied mainly by the secretory pathway (McMichael and Bednarek, 2013; Richter et al., 2014; Boruc and Van Damme, 2015). Adaptations of canonical trafficking mechanisms are, however, required because there is no pre-existing target membrane at the site of cell division to which vesicles can fuse. Instead, membrane deposition is thought to be initiated by 'homotypic' fusion of vesicles (Smertenko et al., 2017). This raises the question of how vesicle fusion is spatially restricted to the site of cell division, instead of it occurring spuriously throughout the whole cell. It has been proposed that vesicles are transported along polarized microtubules to the center of the phragmoplast, a cytoskeletal apparatus that supports cell plate assembly (Euteneuer et al., 1980; Lee et al., 2001; Otegui et al., 2001). Transport may concentrate vesicles locally to enhance fusion rates but whether transport alone can provide the spatial accuracy required to build a straight and flat cell plate is unknown. Recently, we have identified short stretches of antiparallel microtubule overlap at the midzone of phragmoplasts in the moss *Physcomitrella patens* as sites where membrane build-up is initiated (de Keijzer et al., 2017). It remained, however, unclear whether there are specific molecules present at overlaps, which then trigger vesicle fusion locally.

In eukaryotic cells the fusion of transport vesicles with endomembrane compartments and the plasma membrane relies on the combined action of fusion and tethering complexes. The force driving the fusion of a vesicle and its destination membrane is almost universally generated by soluble *N*-ethylmaleimide-sensitive factor attachment receptor (SNARE) complexes, which are typically composed of four membrane-associated proteins (Söllner et al., 1993; Wickner and Schekman, 2008; Südhof and Rothman, 2009). However, tethering – the establishment of the initial physical connection between the two membranes – is orchestrated by a multitude of molecular machinery, often in the form of multimeric protein complexes (Koumandou et al., 2007; Vukašinović and Žárský, 2016). To enable targeted trafficking among the various distinct membrane compartments in eukaryotic cells, membranes acquire different identities that dictate which membrane fusion reactions are allowed. Although the SNARE complex composition bestows some of this specificity (Paumet et al., 2004) other factors, including Rab GTPases (Grosshans et al., 2006; Stenmark, 2009) and the various tethering complexes, play an important role as well (Yu and Hughson, 2010). Indeed, each of the several tethering complexes typically facilitates the docking of vesicles at a specific target membrane (Vukašinović and Žárský, 2016; Yu and Hughson, 2010).

While work in *Arabidopsis* has uncovered much about the composition, trafficking and function of the SNARE complexes involved in fusing cell plate vesicles (reviewed in Müller and Jürgens, 2015; Jürgens et al., 2015), comparatively little is known about the functioning of tethering factors involved. In *Arabidopsis*, both the transport protein particle II (TRAPPII) and exocyst tethering complexes contribute to cell plate biogenesis (Thellmann et al., 2010; Fendrych et al., 2010; Qi et al., 2011; Rybak et al.,

[1]Laboratory of Cell Biology, Wageningen University, Droevendaalsesteeg 1, 6708 PB Wageningen, The Netherlands. [2]Laboratory of Phytopathology, Wageningen University, Droevendaalsesteeg 1, 6708 PB Wageningen, The Netherlands. [3]Department of Plant and Microbial Biology and Zurich-Basel Plant Science Center, University of Zurich, 8008 Zurich, Switzerland.
*Present address: Department of Crop Genetics, John Innes Centre, Norwich Research Park, Norwich NR4 7UH, UK. ‡Present address: Department of Bionanoscience, Kavli Institute of NanoScience, TU Delft, Van der Maasweg 9, 2629 HZ Delft, The Netherlands. §Present address: Laboratory of Phytopathology, Wageningen University, Droevendaalsesteeg 1, 6708 PB Wageningen, The Netherlands.

¶Authors for correspondence (tijs.ketelaar@wur.nl; marcel.janson@wur.nl)

T.K., 0000-0001-9506-7264

Received 13 July 2018; Accepted 2 January 2019

Journal of Cell Science (2019) 132, jcs222430. doi:10.1242/jcs.222430

2014). Both are multimeric protein complexes that function in post-Golgi membrane trafficking (Drakakaki et al., 2012; Fendrych et al., 2010; reviewed by Vukašinović and Žárský, 2016). Interestingly, whereas TRAPPII is associated with the cell plate throughout its formation, the exocyst is present on the cell plate during cell plate initiation and, thereafter, its abundance drops during cell plate expansion and increases again after cell plate attachment (Fendrych et al., 2010; Zhang et al., 2013; Rybak et al., 2014). Nonetheless, the two tethering complexes physically interact and are most likely to function cooperatively during cytokinesis (Rybak et al., 2014). Whereas functional analysis of the TRAPPII complex is expedited by only single genes encoding two unique TRAPPII subunits (Thellmann et al., 2010; Qi et al., 2011), the diverse complement of genes encoding exocyst subunits have made dissecting the role of the exocyst comparatively cumbersome. Nonetheless, several exocyst mutants have been identified that harbor cell plate defects (Fendrych et al., 2010; Wu et al., 2013; Rawat et al., 2017).

Here, to understand whether the exocyst is a cell-plate assembly factor active on microtubule overlaps, we monitored the localization of several GFP-tagged exocyst subunits during cytokinesis in the moss *P. patens*. Although this representative of a basal land plant lineage has seen a similar degree of gene amplification regarding exocyst subunit genes as *Arabidopsis* – albeit with a notable smaller radiation of Exo70 paralogs (Cvrčková et al., 2012) – it features a main haploid phase in its life cycle, which expedited genetic analysis. Since cell plate-assisted cytokinesis is a hallmark of all land plants (Buschmann and Zachgo, 2016) and a comprehensive toolset to study cell division exists for *P. patens* (Yamada et al., 2016), we anticipated that this model plant is particularly useful for studying exocyst functioning in relation to the fusion between cell plate membranes. We show that the exocyst subunit Sec6, but not subunits Sec3 and Sec5, localized to microtubule overlaps at the phragmoplast midzone prior to the arrival of membrane vesicles. The localization of Sec6 depended on the presence and size of the microtubule overlaps. Our findings make the case that, in general, spatial control over homotypic vesicle fusion can be achieved by linking tethering activity to a pre-defined, non-membranous subcellular structure.

RESULTS

The eukaryotic exocyst has been best studied for its role in the targeting and fusion of exocytotic vesicles to the plasma membrane. A key step is thought to be the formation of a fully assembled complex between the vesicle- and plasma membrane-associated subunit subsets (e.g. Yu and Hughson, 2010; Boyd et al., 2004). How exocyst assembly proceeds in absence of a plasma membrane in the context of homotypic fusion is unknown. To characterize assembly dynamics during cytokinesis in *P. patens*, we generated a time-resolved localization map of selected exocyst subunits in protonemal tip cells that exhibit repetitive cell divisions. Sec6 was included in the screen because it is the only exocyst subunit that is represented by a single gene in the moss *P. patens* (Cvrčková et al., 2012). The protein was, therefore, expected to be part of all fully assembled exocyst complexes. Moreover, Sec6 from *Arabidopsis* has been shown to interact with vesicle fusion machinery and might, thus, be an important regulator of cell plate formation (Wu et al., 2013). To investigate whether exocyst complex assembly occurs in sequential steps, we included Sec5 and Sec3 paralogs, which – in yeast – have been proposed to be associated to the vesicle and plasma membrane, respectively (He and Guo, 2009). Sec5 is encoded by four genes and Sec3 by three genes in *P. patens* (Fig. S1) (Cvrčková et al., 2012). To conduct the screen, a GFP-encoding fragment was integrated at the end of the single Sec6 gene, at the end of all three genes encoding Sec3 paralogs, and at the end of the three Sec5 paralogs that are expressed in protonemal tissue and/or in caulonemal and/or chloronemal cells (Ortiz-Ramírez et al., 2016) (Fig. S1A). We started by analyzing the relative abundance of the different isoforms by imaging interphase apical caulonemal cells (Fig. S1B). Image-based assessment of relative protein abundance matched the data available from gene expression databases (Fig. S1A). All investigated exocyst subunits, except the less strongly expressing Sec3c, localized to plasma membrane foci as reported previously, and some – notably Sec6 and Sec5b – were also abundant in the cytoplasm (Fendrych et al., 2013; Zhang et al., 2013; Vukašinović and Žárský, 2016; Bloch et al., 2016; Synek et al., 2017; van Gisbergen et al., 2018). Of those subunits that showed brightest cortical localization, i.e. Sec3a, Sec5b, Sec5d and Sec6 (Fig. S1), fusion proteins were expressed together with mCherry-tagged α-tubulin, such that exocyst localization dynamics could be related to mitotic progression (Fig. S1, Fig. 1A). All selected exocyst subunits and, additionally, the established cell plate membrane marker SCAMP4 (de Keijzer et al., 2017) were imaged throughout cell division. The onset of anaphase was used as temporal reference to aid the mutual comparison of arrival times at specific cytokinetic structures (Fig. 1A, Movie 1).

The selected exocyst subunits showed disparate localization patterns during cell division. Sec3a and Sec5b localized to the phragmoplast midzone during cell plate initiation (Fig. 1A, Movie 1). Unlike the exocyst subunits studied in *Arabidopsis* (Fendrych et al., 2010; Zhang et al., 2013; Rybak et al., 2014), no sharp drop in intensity occurred during cell plate expansion. However, similar to the observations in *Arabidopsis*, the amount of Sec3a and Sec5b on the new wall facet transiently increased after cell plate attachment, while that of Sec5d deviated from this localization and was absent from the cell plate until late cytokinesis. Moreover, Sec6 was detected already at the center of the division apparatus from spindle formation onwards (Fig. 1A, white arrowheads; Movie 1). Unlike the other studied exocyst subunits, the intensity of Sec6 at the phragmoplast midzone peaked during cell plate initiation and expansion, and dropped after cell plate attachment. Imaging of Sec6 in conjunction with FM4-64, an amphiphilic dye for the endomembrane system, showed that a distinct pattern of bright Sec6 sections was visible in the phragmoplast midzone before initial deposits of cell plate membrane appeared ∼2 min after anaphase onset (Fig. 1C, Movie 2; de Keijzer et al., 2017). Interestingly, all four selected subunits were already stably associated with the cell cortex before cell plate attachment at a site where the cell division plane intersected with the parental cell wall (Fig. 2A,B). To our knowledge such cortical localization pattern has not been observed during cytokinesis for any labeled subunit in *Arabidopsis* (Fendrych et al., 2010; Zhang et al., 2013; Rybak et al., 2014). The early cortical labeling was punctate, with several puncta making up a 2–3 µm wide band that formed a continuous ring at the cell cortex (Fig. 2A). The band was mobile on the cortex until cell plate attachment and its movement was synchronous with rotation of the phragmoplast in these cells (Fig. 2B,D).

To further characterize the observed differences in localization, we identified those moments – with respect to anaphase onset – at which subunits first became visible at the phragmoplast midzone and the cortex (Figs 1B and 2C). This analysis showed that all studied subunits arrived at the cortex at around the same time (5–10 min post anaphase onset). The average time of arrival at the phragmoplast midzone, however, diverged for the studied subunits. Sec6 was already visible when the spindle midzone transformed into the phragmoplast midzone at the onset of anaphase. Sec3a

Journal of Cell Science (2019) 132, jcs222430. doi:10.1242/jcs.222430

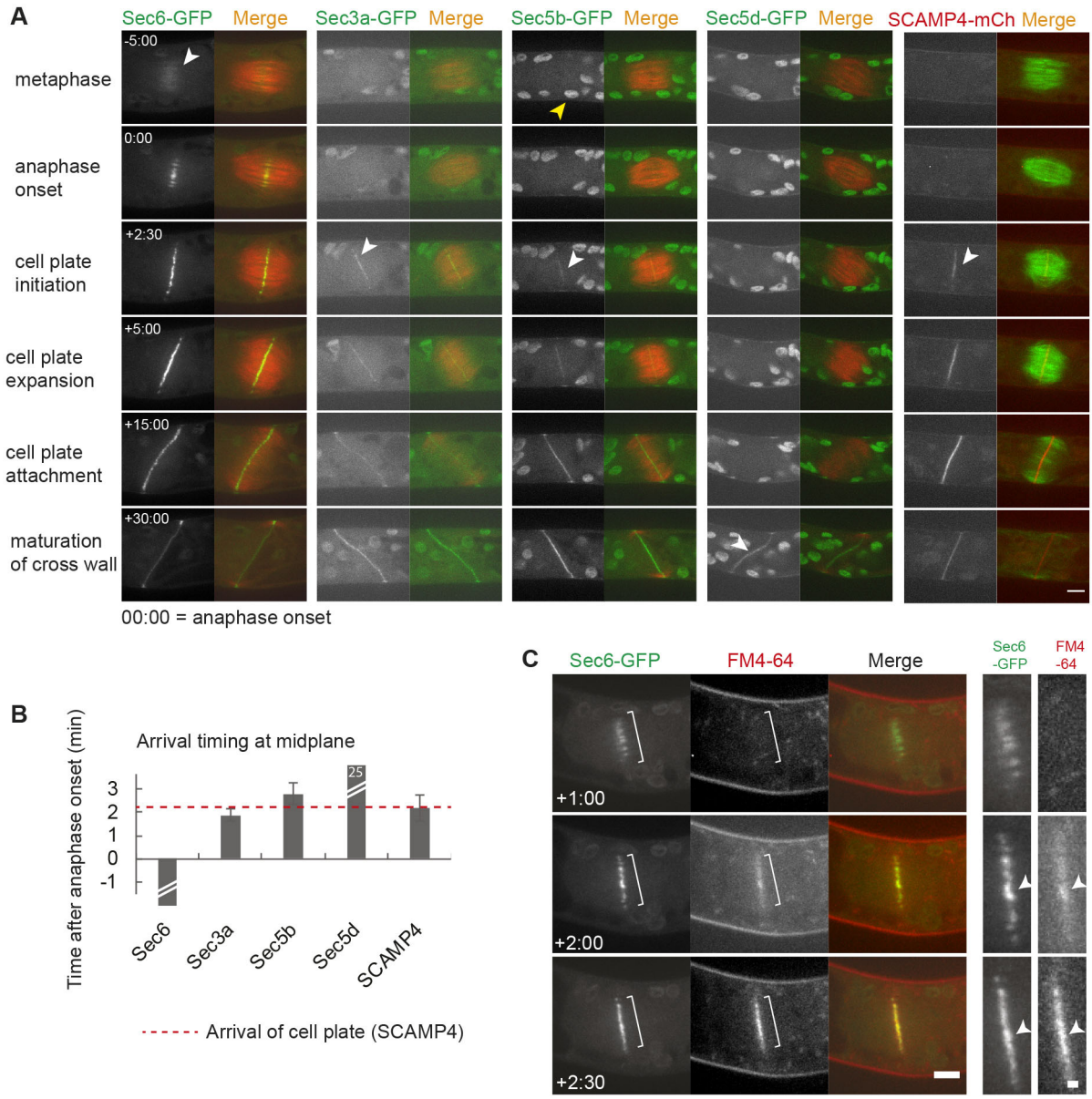

Fig. 1. Localization survey of a subset of *Physcomitrella patens* exocyst subunits during cell division. (A) Localization of exocyst subunits Sec6, Sec3a, Sec5b and Sec5d during cell division visualized in caulonemal apical cells expressing mCherry-α-tubulin (red in merged image) and a GFP-tagged version of the indicated exocyst subunit. The progression of cell plate and phragmoplast development, visualized with cell plate marker SCAMP4 (de Keijzer et al., 2017) and GFP-α-tubulin, is depicted on the right as a reference. Time after anaphase onset (*t*=0) is indicated (min:sec). Localization to the phragmoplast midzone is indicated by white arrowheads. A typical autofluorescent chloroplast is indicated by a yellow arrowhead. Images are maximum *z*-projections of three confocal planes spaced 0.5 µm apart. Scale bar: 5 µm. (B) Bar graph showing the average appearance time of GFP-tagged exocyst subunits at the phragmoplast midzone compared to that of cell plate membrane (SCAMP4-mCherry, dashed line). The cut bar for Sec6 indicates that it appeared on the spindle from prophase onwards, the timing of which was not quantified (see Fig. 1A). Error bars indicate ±s.d. Averages were obtained from *n*=4 cells (Sec6 and Sec3a), *n*=5 cells (Sec5b and Sec5d) or *n*=8 cells (SCAMP4). (C) Early cell plate membrane accumulation visualized in a dividing cell expressing Sec6-GFP stained with FM4-64 membrane dye. Time with respect to anaphase onset (*t*=0) is indicated (min:sec). The bracketed areas are shown magnified on the right. Arrowheads mark membranous material accumulating at Sec6-labeled sites. Images are maximum *z*-projections of three confocal planes spaced 0.5 µm apart. Scale bars: 5 µm (overview images); 1 µm (magnified images).

and Sec5b, however, appeared simultaneously with the initial membrane accumulations, and Sec5d only appeared ∼23 min later (Fig. 2, Movies 1, 8, 9). The more weakly expressing paralogs Sec3b-GFP and Sec5a-GFP also appeared at the midzone at the time of initial membrane accumulation (Movie 2). Thus, whereas sharing localization at the cortex and late cell plate with the other studied exocyst subunits, Sec6 exhibited localization to the phragmoplast and spindle midzones apparently independent of the other studied exocyst complexes and membrane compartments.

The early localization pattern of Sec6 showed strong resemblance to sites at which microtubules from opposite poles form antiparallel overlaps in the spindle and phragmoplast midzone (Ho et al., 2011; Kosetsu et al., 2013; de Keijzer et al., 2017). To investigate their interdependency, we generated a moss line expressing Sec6-mCherry together with a Citrine-tagged version of the antiparallel microtubule bundling protein MAP65 (Kosetsu et al., 2013). Sec6 localization, indeed, closely followed the distribution of MAP65-Citrine labeled regions (Fig. 3, left panels; Movie 3). Strikingly, this behavior was

Journal of Cell Science (2019) 132, jcs222430. doi:10.1242/jcs.222430

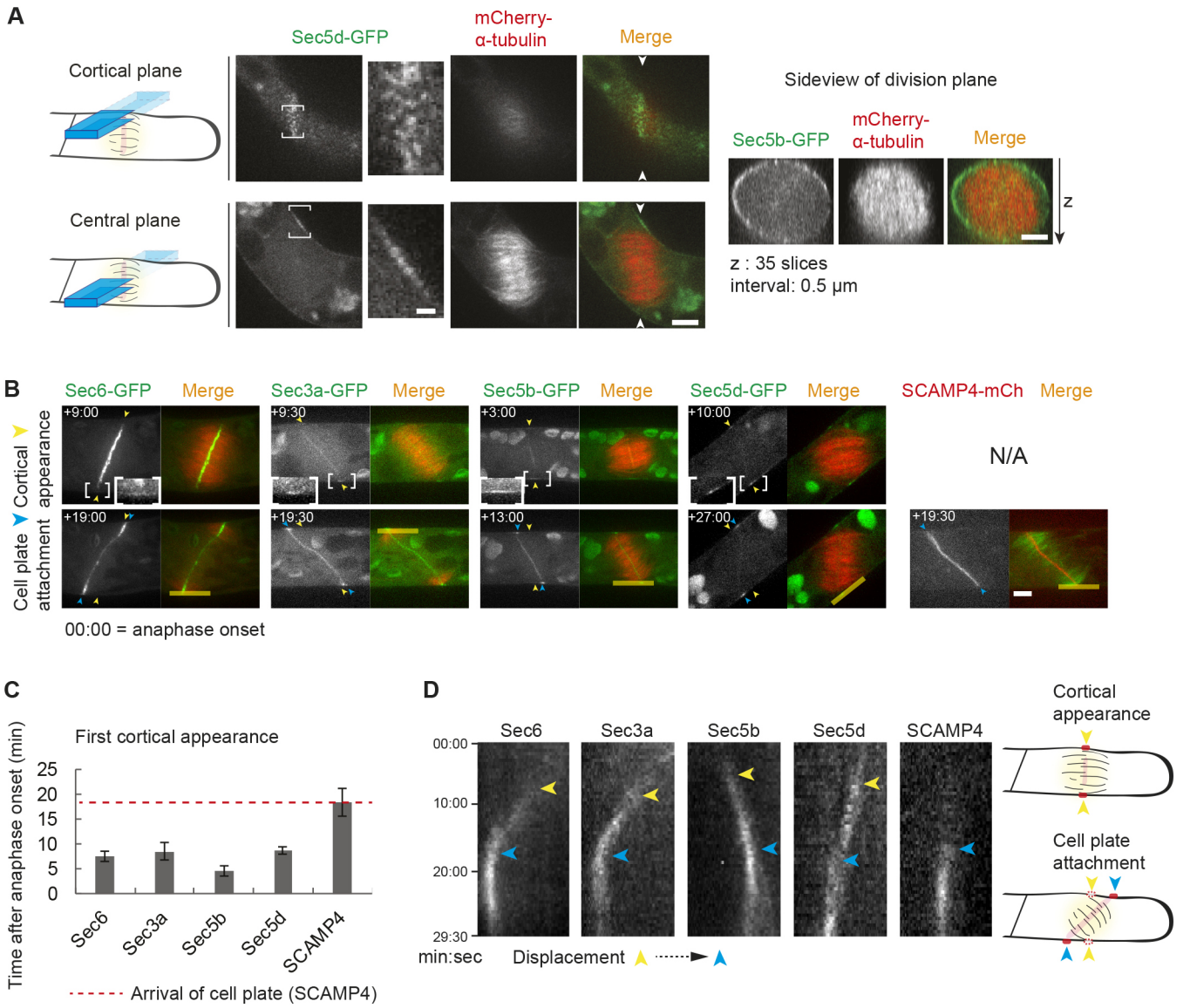

Fig. 2. Exocyst subunits arrive to cortical membrane prior to cell plate insertion. (A) Cortical localization of the exocyst during cell division visualized in a cell expressing Sec5d-GFP and mCherry-α-tubulin at a single cortical and a central confocal plane (illustrated on the left). A detailed view of the Sec5d-GFP signal indicated by the brackets is shown. A sideview of the division plane (marked with arrowheads) is depicted on the right. This sideview was generated with 35 *z*-slices using interpolation to obtain a 1:1 pixel aspect ratio. Scale bars: 5 µm (overview and sideview images), 1 µm (magnified images). (B) Snapshots of dividing caulonemal cells expressing exocyst subunit-GFP (Sec6, Sec3a, Sec5b and Sec5d) and membrane marker SCAMP4-mCherry. Microtubules labeled with mCherry-α-tubulin or GFP were used as a temporal reference. Images are maximum *z*-projections of 3 planes spaced 0.5 µm apart acquired in the central plane. Images were recorded with 30 s interval. Time with respect to anaphase onset (*t*=0) is indicated (min:sec). Scale bar: 5 µm. The time point each subunit first appeared at the cortex is indicated by yellow arrowheads in the upper panels, which have been copied to the lower panels. The bracketed areas are shown in detail. The final localization of each subunit in the cortex at the moment of cell plate insertion is indicated by blue arrowheads in the lower panel. (C) Bar graph showing the average appearance time of GFP-tagged exocyst subunits at the cell cortex compared to that of cell plate membrane (SCAMP4-mCherry, dashed line). Error bars indicate ±s.d. Averages were obtained from *n*=4 cells (Sec6 and Sec3a), *n*=5 cells (Sec5b and Sec5d) or *n*=8 cells (SCAMP4). (D) Kymographs of exocyst subunits and SCAMP4 generated along the parental plasma membrane, as indicated by the yellow lines depicted in B. A region of 0.67 µm perpendicular to the line was used to calculate average intensity. Yellow arrowheads mark the timing of arrival; blue arrowheads indicate the timing of cell plate attachment.

even visible during prophase, when the nuclear envelope is still intact and no bipolar spindle has yet formed (Fig. 3, arrowheads). We have previously generated cells lacking the regulator of microtubule dynamics Kin4-Ic (Δ*kin4-Ic* cells), which show delayed shortening of microtubule overlaps at anaphase onset (de Keijzer et al., 2017). In this genetic background a similarly strong colocalization of MAP65 and Sec6 was observed during prophase and spindle stages. The width of the Sec6 patches after anaphase onset was larger in Δ*kin4-Ic* cells, which is in accordance with the larger overlaps. As cytokinesis progressed, Sec6 increasingly localized to only the central region of MAP65, resembling membrane depositions that also gradually became more confined to overlap centers (Fig. 3, arrows in right panel; Movie 3; de Keijzer et al., 2017). This behavior was best visible before overlaps shortened in Δ*kin4-Ic* cells, i.e. ∼5 min after anaphase onset. Thus, Sec6 localizes to MAP65 regions but, after cell plate initiation, other factors might additionally affect its localization.

Journal of Cell Science (2019) 132, jcs222430. doi:10.1242/jcs.222430

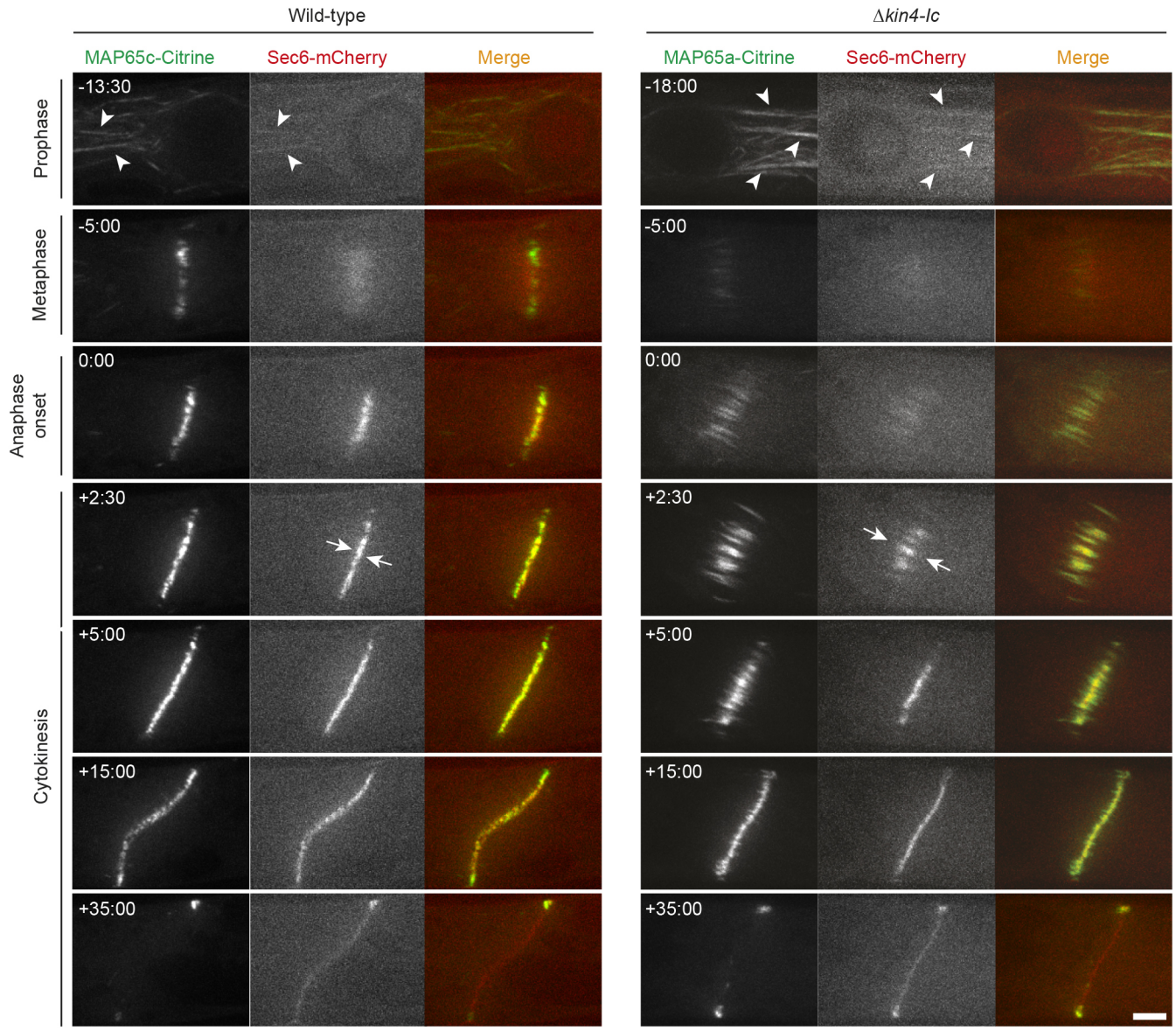

Fig. 3. Exocyst subunit Sec6 partially colocalizes with MAP65 on antiparallel microtubule overlaps. Caulonemal cells expressing citrine-labeled MAP65 and Sec6-mCherry in a wild-type (left) and Δ*kin4-Ic* (right) genetic background imaged throughout mitosis. MAP65-labeled microtubule bundles present during prophase that show concomitant Sec6 labeling are marked with arrowheads. Arrows highlight the difference in width of the Sec6-labeled and MAP65-labeled zones during early cytokinesis. Time with respect to anaphase onset (*t*=0) is indicated (min:sec). Images are maximum *z*-projections of three confocal planes spaced 0.5 µm apart. Scale bar: 5 µm.

To further understand the extent to which the presence of microtubule overlaps is a prerequisite for the localization of Sec6 during cytokinesis, we silenced the three MAP65 genes expressed in protonema. Earlier studies have demonstrated that, upon knockdown of MAP65, antiparallel microtubule overlap formation in the phragmoplast is severely compromised, ultimately leading to phragmoplast collapse and cytokinesis failure. Nonetheless, during early cytokinesis cell plate membrane does aggregate and phragmoplast microtubules remain organized as two opposing sets (Kosetsu et al., 2013). Whereas in control cells Sec6-GFP appeared to be regularly distributed over the division plane during early cytokinesis, in MAP65-silenced cells Sec6-GFP formed discontinuous patterns (Fig. 4; Movie 4). There was no obvious correlation between the appearance of gaps in the Sec6 localization pattern and the presence of microtubules; areas devoid of Sec6 were visible both in regions populated and unpopulated by microtubules (Fig. 4B). Localization of Sec6 to the phragmoplast midzone, therefore, not just correlates with the presence of bipolar microtubules but requires an ordered array of microtubule overlaps.

A physical interaction between Sec6 and Sec1/Munc18 (SM) family protein KEULE has been proposed to be an important regulatory step in cytokinetic vesicle fusion in *Arabidopsis* (Wu et al., 2013). KEULE contributes to fusion by preventing the important cytokinetic SNARE-component KNOLLE from refolding into its closed, non-fusion-competent conformation, thereby allowing the formation of fusogenic trans-SNARE complexes among vesicles delivered to the cell plate (Park et al., 2012; Karnahl et al., 2017; Jürgens et al., 2015). Whether the Sec6 interaction regulates this specific activity is presently unknown. Nonetheless, cytokinesis defects were found in Sec6 mutants that resemble these encountered in plants lacking KEULE (Wu et al., 2013; Assaad et al., 1996), hinting that a cooperative Sec6-KEULE interaction regulates

Journal of Cell Science (2019) 132, jcs222430. doi:10.1242/jcs.222430

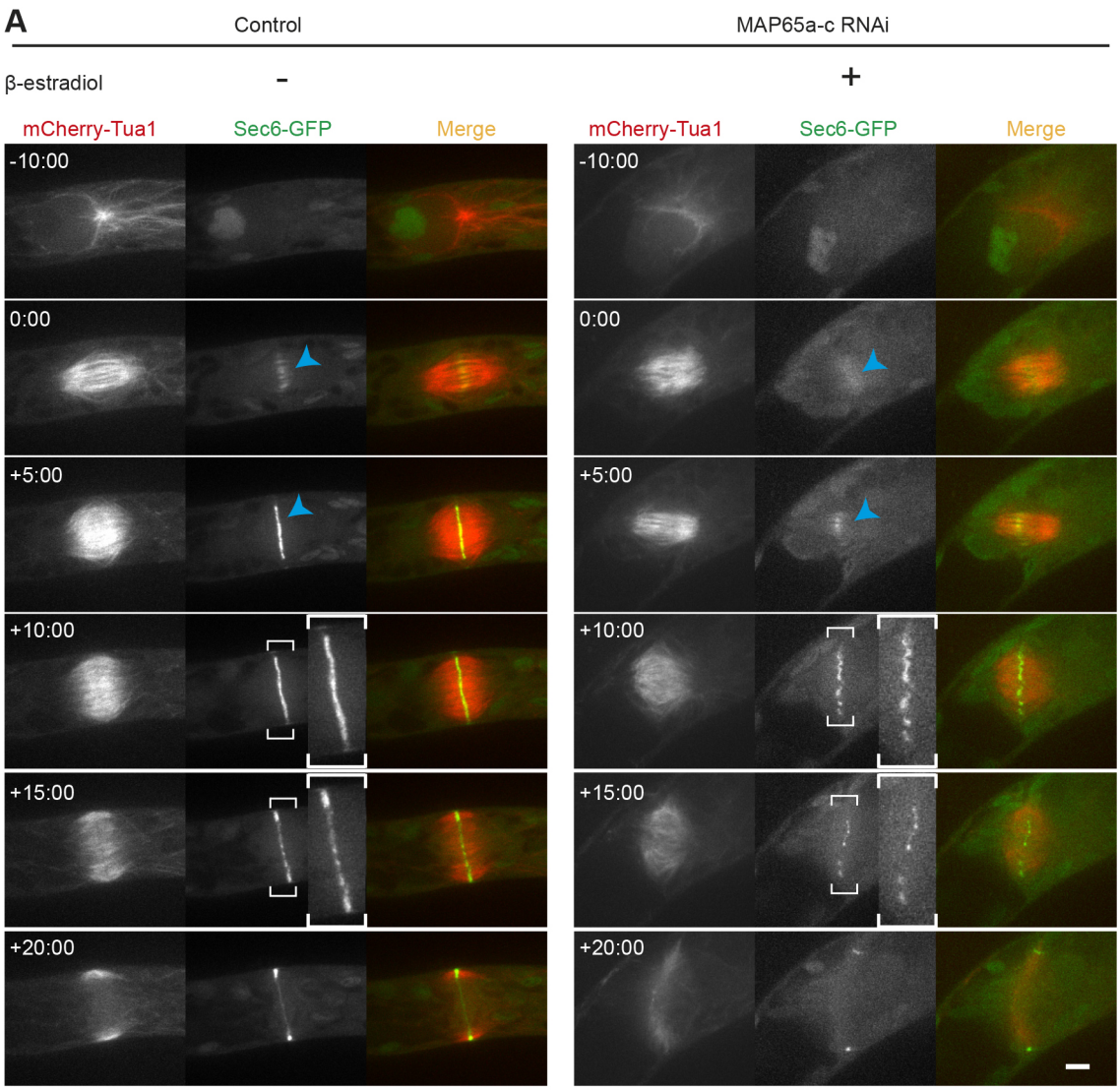

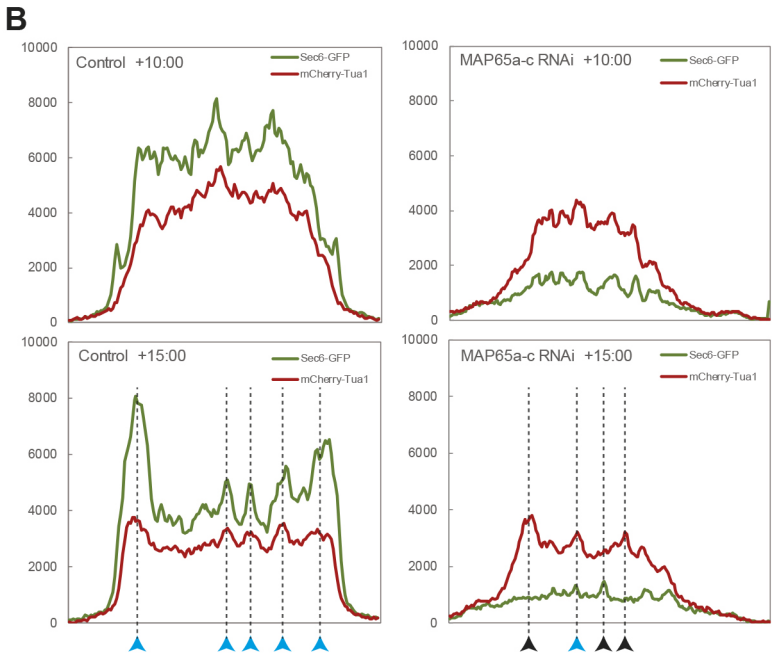

Fig. 4. See next page for legend.

Journal of Cell Science (2019) 132, jcs222430. doi:10.1242/jcs.222430

Fig. 4. The localization of exocyst subunit Sec6 to antiparallel microtubule overlaps depends on overlap length and presence of MAP65. (A) Time sequence of dividing caulonemal cells expressing Sec6-GFP and mCherry-α-tubulin (mCherry-Tua1) after RNAi of MAP65a, b and c (MAP65a-c) under non-induced (control) or induced conditions. Arrowheads mark the accumulation of Sec6 to the phragmoplast midzone during early cytokinesis. Bracketed areas at times +10:00 and +15:00 indicate the midzone during a later stage of cytokinesis and are magnified in the insets. Time with respect to anaphase onset (*t*=0) is indicated (min:sec). Images are maximum *z*-projections of three confocal planes spaced 0.5 µm apart. Scale bar: 5 µm. (B) Fluorescence line plots, 15 pixels in width, of Sec6 and microtubule signals as shown in A parallel to the phragmoplast midzone. Blue arrowheads indicate positions at which both tubulin signals and Sec6 signals have a local maximum. Black arrowheads indicate positions at which only one of the signals has a local maximum. The lack of correlation between signals was especially apparent 15 min after anaphase onset.

cytokinesis. On the basis of these findings, we hypothesized that Sec6 on overlaps in moss regulates vesicle fusion activity in space through an interaction with KEULE. In search of a gene homologous to *KEULE*, we identified seven loci in the *P. patens* genome that are predicted to encode SM family proteins. Of those loci, two comprised genes with a predicted exon number identical to that of the *Arabidopsis KEULE* (*AtKEULE*) gene, i.e. Pp3c17_24130 and Pp3c16_570; and their expected gene products exhibited an overall similarity to that of AtKEULE that was at least twice as high as for the other predicted SM genes (Fig. 5A). Analysis of gene expression levels revealed that the gene encoded at locus Pp3c17_24130 was ubiquitously expressed in moss tissues, whereas the other gene (at Pp3c16_570) was only expressed in rhizoids (Fig. 3A and Fig. S2) (Ortiz-Ramírez et al., 2016). We, therefore, focused on the former gene and tentatively named it *P. patens* KEULE (*PpKEULE*). Since the position of introns in genes contains information on the evolutionary trajectory of the gene family they belong to (e.g. Rogozin et al., 2003; Garcia-España et al., 2009; Javelle et al., 2011), we compared the intron–exon structure between *AtKEULE* and *PpKEULE*. The intron positions were highly similar for both species (Fig. 5B). Introns in the *PpKEULE* gene were slightly longer; however, this is in line with increased average intron length in moss compared to that of *Arabidopsis* (Rensing et al., 2005). The concurrent intron–exon structure of the genes of both species indicates that *PpKEULE* is likely to be orthologous to *AtKEULE*.

In *Arabidopsis*, the interaction domain of KEULE with Sec6 was narrowed down to a C-terminal portion of the protein designated C1 (Wu et al., 2013). The high degree of sequence conservation allowed us to delineate the same domain in PpKEULE and test it for its ability to interact with Sec6. In a reciprocal yeast two-hybrid assay with *P. patens* Sec6, KEULE (PpKEULE) and the C1 domain of KEULE (PpKEULE-C1), we found a strong interaction between Sec6 and both PpKEULE and PpKEULE-C1 when Sec6 was fused to the activation domain of the Gal4 transcription factor. When Sec6 was fused to the DNA-binding domain of Gal4 only a weak interaction with the PpKEULE-C1 domain was found (Fig. 5C). Possibly, in this case, the binding partners are in a less favorable configuration to reconstitute Gal4 function since a similar result was reported for the interaction of *Arabidopsis* proteins (Wu et al., 2013). Because PpKEULE interacts with Sec6 in a fashion indistinguishable from that of its ortholog in *Arabidopsis*, the two proteins might form a conserved module regulating cell plate membrane fusion. To investigate where and when in *P. patens* Sec6 and PpKEULE might interact, we visualized Sec6-mCherry together with endogenous PpKEULE tagged with GFP (Fig. S3). We chose to fuse GFP to the C-terminal end, since this yielded a functional fusion protein for AtKEULE (Steiner et al., 2016). Although absent from Sec6-labeled regions during prophase and metaphase, PpKEULE-GFP became rapidly enriched at the site of Sec6-mCherry at the onset of cytokinesis around the time that localized membrane deposition is first observed at overlaps (Fig. 5D; Movie 5). During radial expansion of the phragmoplast, appearing sites of Sec6 localization at the leading zone, which are likely to correspond with newly formed microtubule overlaps with yet little accumulated vesicles (de Keijzer et al., 2017), had low PpKEULE-GFP signal associated (Fig. 5D, arrowheads). At the cortical zone marked by the labeled exocyst subunit no corresponding PpKEULE signal was found (Fig. 5D, arrow). Taken together, the colocalization pattern suggested that physical association between Sec6 and PpKEULE in a cytokinetic context is both spatially and temporally regulated.

To investigate the functional importance of Sec6 for correct KEULE localization and cell plate assembly in general, we sought out ways to reduce or abolish cellular Sec6 levels. We failed to isolate a Sec6 knockout mutant, suggesting that Sec6 is an essential protein for cell proliferation – as it has been reported in RNA interference (RNAi) studies by van Gisbergen et al. (2018). We, therefore, introduced inducible small interfering RNA (siRNA) of Sec6 in cells expressing either the cell plate membrane marker SCAMP4-mCherry or PpKEULE-GFP. RNAi of Sec6 caused an ∼80% reduction of moss colony expansion over a 5-day growth period and an absence of caulonemal cells (Fig. S4A,C). Continuation of colony expansion suggested that some functional exocyst complexes remain present after initiating RNAi. This was in agreement with an incomplete (∼3-fold) reduction of transcript levels after RNAi (Fig. S5B). When using RNAi in which different regions of the *Sec6* gene were targeted in chloronemal cells, we reproducibly found a more-bulbous tip shape, suggesting that exocyst functioning in polarized tip growth was severely disrupted but not completely abolished (Figs S4C and S6). Three days after induction of knockdown using RNAi, the final cell walls separating two daughter cells showed several morphological defects (Fig. S4D). Incomplete cytokinesis could, however, not be concluded without ultrastructural analysis of the formed cell plates. To understand whether defects arose due to exocyst malfunctioning during cell plate initiation and expansion, we observed cells expressing SCAMP4-mCherry as a membrane marker throughout cytokinesis (Fig. 6A). Although the time of initial membrane appearance was similar, the rate at which membrane material accumulated was delayed after initiating RNAi (Fig. 6B and Movie 6). RNAi experiments, thus, suggested that reduction of Sec6 functioning at the midzone decreased membrane build-up during early cytokinesis, a time at which Sec6 levels peaked in unperturbed cells (Fig. 1A). Surprisingly, the velocity of cell plate expansion appeared similar under both induced and non-induced conditions (Fig. 6D). To test whether silencing of Sec6 affects KEULE levels at the phragmoplast midzone, we imaged PpKEULE-GFP after initiation of RNAi. A delay in the recruitment of PpKEULE-GFP to the midzone was observed after induction with similar dynamics as SCAMP4-mCherry (Fig. 6E,F; Movie 7). This suggested that KEULE accumulation to the phragmoplast midzone was, at least partly, dependent on Sec6, which is in agreement with the observed interaction between KEULE and Sec6 (Fig. 5).

DISCUSSION

Our cytokinesis-oriented localization screen of exocyst subunits in moss revealed two localization patterns that have not been previously described in plants. First, exocyst subunits localized to MAP65-labeled regions in the midzone of the spindle and phragmoplast. Second, they formed a cortical ring prior to cell plate attachment.

Journal of Cell Science (2019) 132, jcs222430. doi:10.1242/jcs.222430

A

v1.6 locus identifier	v3.1 locus identifier	% identity with AtKEULE	# of exons	expressed in protonema
Pp1s468_8	Pp3c17_24130	54.50%	21	+
Pp1s144_47	Pp3c16_570	49.53%	21	-
Pp1s33_94	Pp3c18_21360	23.60%	13	+
Pp1s391_41	Pp3c12_11250	21.04%	4	-
Pp1s188_85	Pp3c4_5220	20.77%	4	+
Pp1s26_105	Pp3c17_5740	18.09%	22	+
Pp1s203_96	Pp3c9_21860	16.44%	10	+

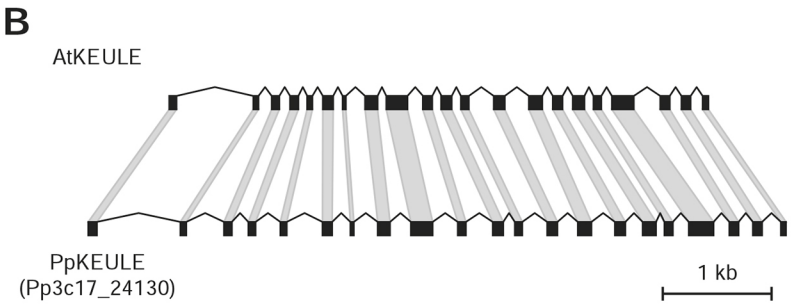

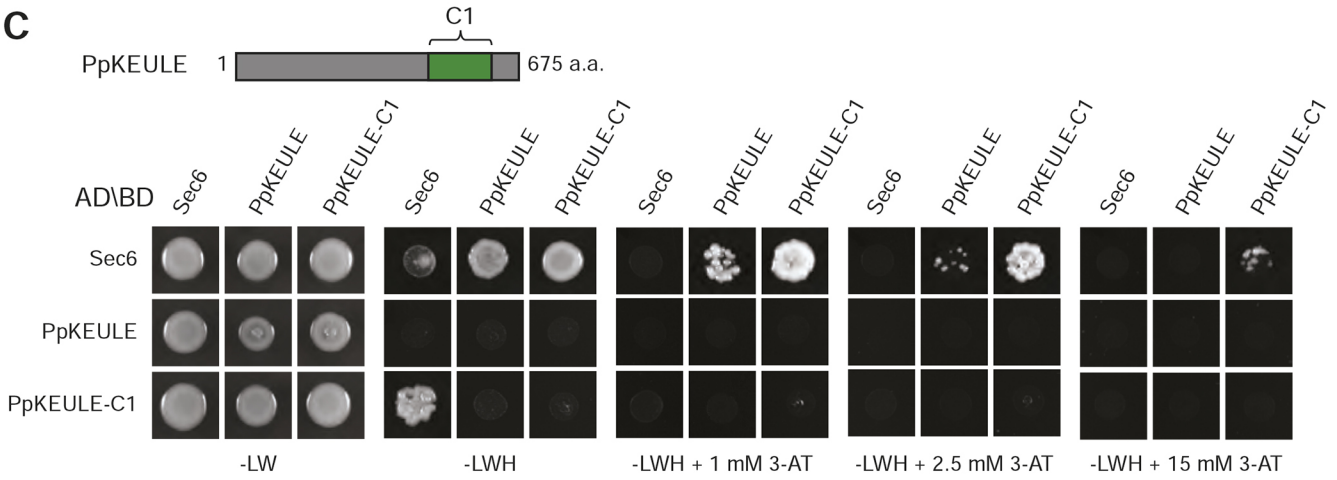

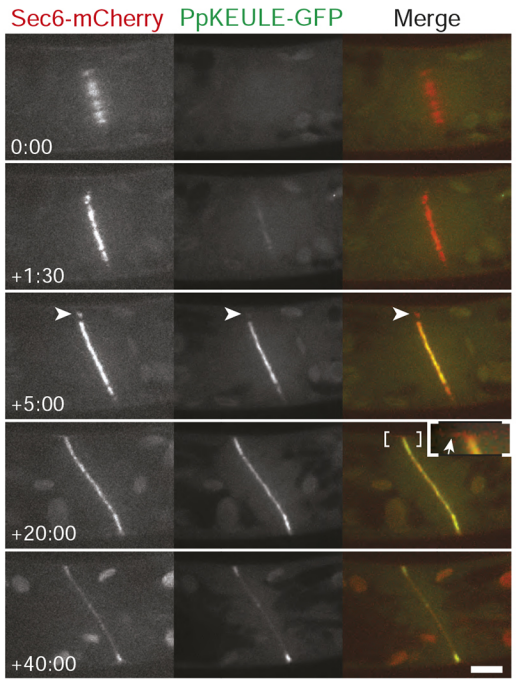

Fig. 5. Identification of a *P. patens* KEULE ortholog that physically interacts with Sec6 and colocalizes at the phragmoplast midzone during cell plate formation. (A) List of loci that putatively encode Sec1/Munc18-like (SM) family proteins and their similarity (% identity) to the cytokinetic Sec1 protein AtKEULE at protein level. The locus identifiers for two versions (v1.6 and v3.1 of Cosmoss database, http://www.cosmoss.org) of the *P. patens* genome assembly are given. For each predicted gene the number of exons and the presence of indicators of gene expression in protonemal tissue are given. (B) AtKEULE and the putative *P. patens* ortholog (PpKEULE) expressed in protonema. (C) Yeast two-hybrid interaction assay of Sec6, PpKEULE and the PpKEULE C1 domain (illustrated at the top). Sec6, PpKEULE and PpKEULE C1 domain proteins were fused to the Gal4 activating and binding domains (AD/BD) and their different combinations coexpressed in yeast strains that were then tested for growth on reporter medium lacking Leu and His (–LW), or medium lacking Leu, Trp and His (–LWH) alone or in combination with increasing amounts (1, 2.5 or 15 mM) of the competitive inhibitor 3-AT. (D) Sec6 and PpKEULE visualized together throughout cell division in a cell expressing Sec6-mCherry and PpKEULE-GFP. The arrowheads indicate Sec6-labeled regions at the expanding edge of the phragmoplast, showing less associated KEULE-GFP compared to the central regions. An enlarged view of the bracketed area is depicted in the inset, in which the arrow points to Sec6 located at the cortex without an associated PpKEULE-GFP signal. Images are maximum *z*-projections of three confocal planes spaced 0.5 µm apart. Scale bar: 5 µm.

Interestingly, the two localization patterns overlapped in time yet differed in subunit composition. In the midzone, Sec6 arrival preceded that of Sec5 and Sec3 homologs, although this was not evident for the cortical localization. The systematic design of the conducted screen, thus, provides some of the clearest evidence to date for sequential assembly of the exocyst complex. So, although biochemical purification and live cell data show that the eight exocyst subunits in yeast form a stable complex, our work shows that subunits can as well have individual localization patterns (Hála et al., 2008; Heider et al., 2016; Picco et al., 2017).

In most plant cells a cortical ring of microtubules, the preprophase band (PPB), is thought to demarcate a functionalized section of the cortex, called the cortical division zone (CDZ), to which cell plate expansion is directed during cytokinesis (van Damme, 2009; Müller et al., 2009; Stöckle et al., 2016). Known components of the CDZ do, however, assemble into ring-like structures in mutants that are unable to form a PPB (Spinner et al., 2010). Other cells, including moss protonemal cells, lack a PPB altogether but cytokinesis does involve the formation of a cortical band with established CDZ components, including myosins and

Journal of Cell Science (2019) 132, jcs222430. doi:10.1242/jcs.222430

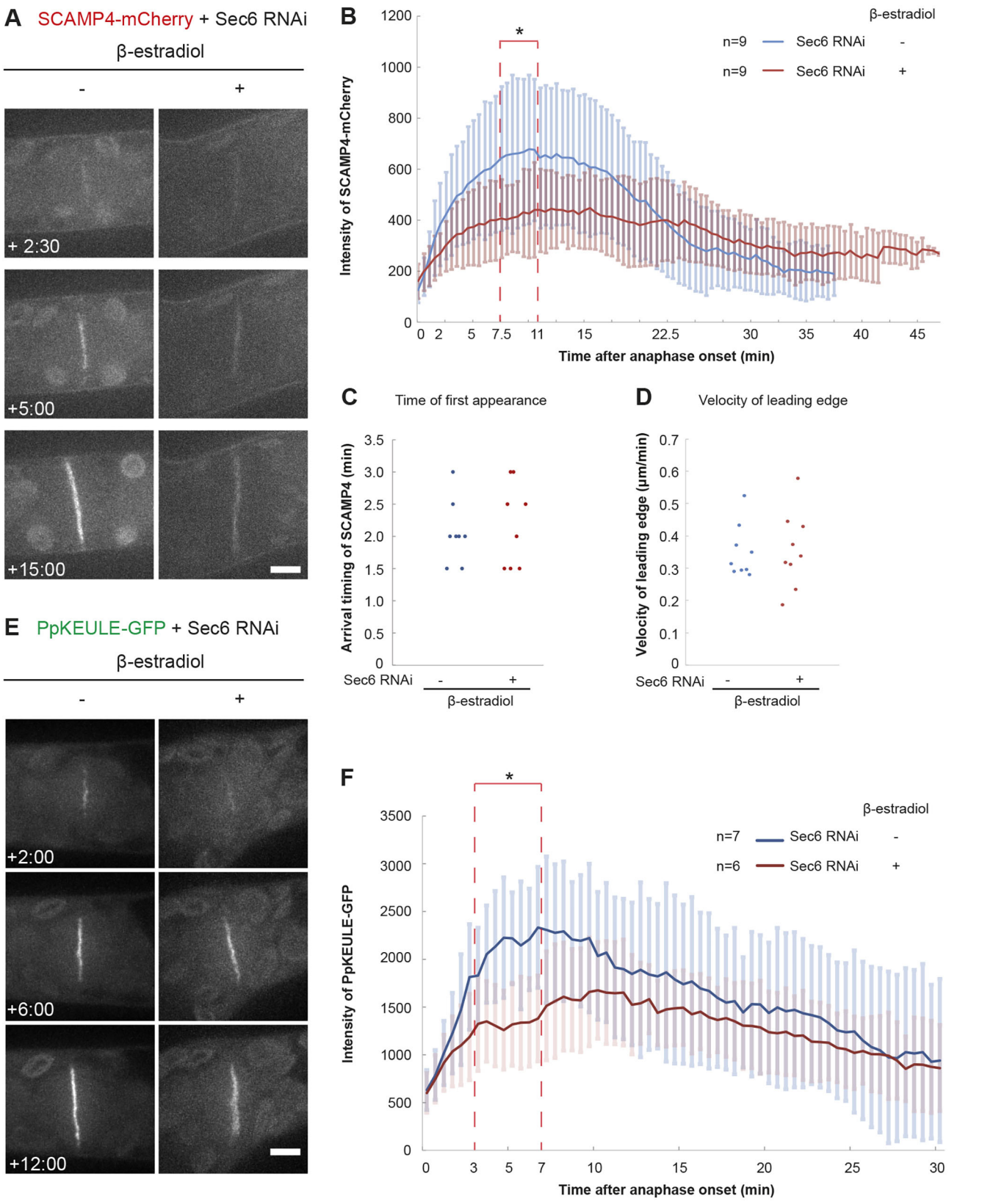

Fig. 6. See next page for legend.

kinesins, prior to cell plate attachment (Schmiedel et al., 1981; Doonan et al., 1985; Otegui and Staehelin, 2000; Hiwatashi et al., 2008; Wu et al., 2011; Nakaoka et al., 2012; Miki et al., 2014; Wu and Bezanilla, 2014; Lipka et al., 2014; Schaefer et al., 2017; Kosetsu et al., 2017). Given the early cortical localization of the exocyst observed in moss, it will be interesting to find out whether

Journal of Cell Science (2019) 132, jcs222430. doi:10.1242/jcs.222430

Fig. 6. Initial recruitment of membrane materials and PpKEULE is reduced upon Sec6 silencing. (A) Snapshots of a dividing cell showing the mCherry-tagged membrane marker protein SCAMP (SCAMP4-mCherry) in response to RNAi of *Sec6* induced by treatment with β-estradiol. The intensity of SCAMP4-mCherry is depicted at the same contrast settings. Time with respect to anaphase onset (*t*=0) is indicated (min:sec). Images are maximum *z*-projections of three planes spaced 0.5 µm apart acquired in the central plane. Scale bar: 5 µm. (B) Average intensity of SCAMP4-mCherry quantified throughout cytokinesis; ±s.d. is given for each time point. **P*<0.05 (significant difference between control and *Sec6* RNAi during 7.5–11 min, using Student's two-tailed *t*-tests). (C) Onset of membrane arrival in *Sec6* RNAi background with or without treatment with β-estradiol. Anaphase onset is set up as *t*=0. *n*=8 for both treatments. (D) Expansion rate of the cell plate in a *Sec6* RNAi background with or without induction. *n*=8 for both control and *Sec6* RNAi. (E) Localization of PpKEULE-GFP in a *Sec6* RNAi background. Representative snapshots are shown in the early, middle and late phase of cytokinesis. Images are maximum *z*-projections of three planes spaced 0.5 µm apart, acquired in the central plane. KEULE-GFP is depicted in RNAi and control cells using identical contrast settings. Scale bar: 5 µm. (F) Average PpKEULE-GFP intensity throughout cytokinesis; ±s.d. is given for each time point. **P*<0.05 (significant difference between control and *Sec6* RNAi for 3–7 min, using Student's two-tailed *t*-tests).

exocyst and vesicle trafficking have a role in the establishment or maintenance of the CDZ in absence of a PPB, or whether its function is limited to attachment of the cell plate. Analogies may be present in fission yeast cytokinesis, where exocyst localization and vesicle fusion to the division site appear to precede ingression of the cleavage furrow (Wang et al., 2016). It is surprising that no exocyst subunits have been reported as components of the CDZ in higher plants (Vukašinović and Žárský, 2016; Boruc and van Damme, 2015). Characterization of exocyst localization in plants is, however, impeded by the large number of subunits homologs, particularly the Exo70 subunit.

Local accumulations of exocyst subunits were first described for their role in polarized exocytosis at the plasma membrane (TerBush and Novick, 1995; Hazuka et al., 1999). However, exocyst subunits also localize to internal membrane compartments to assist in autophagosome formation (Kulich et al., 2013; Bodemann et al., 2011). Moreover, in budding and fission yeast it has been demonstrated that the deliberate targeting of exocyst subunits to mitochondria reroutes cellular trafficking towards these organelles (Luo et al., 2014; Wang et al., 2016). These observations lead us to propose that, in moss, a local pool of exocyst subunits on microtubule overlaps stimulates the immobilization and fusion of vesicles to initiate cell plate assembly. However, in all mentioned examples, local pools of exocyst subunits are bound to membranes, whereas – in our study – Sec6 localized to non-membranous microtubule overlaps. It is, therefore, not self-evident how Sec6 on overlaps can initiate membrane-membrane interactions necessary for homotypic vesicle fusion, even when it seeds the assembly of a complete exocyst complex. Possibly, vesicles arrive at the phragmoplast midzone in a fusion-incompetent state and formation of enabled SNARE complexes involves interactions between SNAREs, KEULE and exocyst subunits. In fact, Sec6 appears to be at the center of an interaction network because Sec6 homologs in diverse systems interact with both SNARE and SM proteins separately from other exocyst subunits (Hong and Lev, 2014; Hashizume et al., 2009; Morgera et al., 2012; Dubuke et al., 2015; Sivaram et al., 2005, 2006). Cytosolic levels of Sec6 might be insufficient to establish these regulatory molecular interactions on vesicles, whereas concentrated Sec6 on overlaps could generate a local pool of fusion-competent vesicles near overlaps. Our finding, thus, suggests how vesicle fusion activity may be regulated in space, an aspect that – so far – remains unresolved. Interestingly, PpKEULE does not localize to cortical exocyst subunits prior to cell plate attachment. It might, thus, be exclusively required to regulate vesicle fusion activity in the phragmoplast midzone during cytokinesis.

Unique about Sec6 during moss cytokinesis was its initial localization to the phragmoplast midzone in complete absence of membranes. It is possible that other exocyst subunits share this localization pattern but not Sec5 and Sec3 – which arrived later, around the time of initial membrane accumulation. Colocalization of MAP65 and Sec6, at a stage during which MAP65 is localized to visible regions of microtubule overlap in the phragmoplast midzone (Fig. 3; Kosetsu et al., 2013), demonstrated that Sec6 first associates along microtubule overlaps. Observations in mammalian cells suggest that microtubule overlaps have a more common role in controlling vesicular transport. Through interaction with centralspindlin the protein MICAL3 first localizes to the spindle midzone starting in anaphase and later targets Rab8a-positive vesicles to the midbody (Liu et al., 2016). Centralspindlin does, however, transfer from microtubule overlaps to an adjacent exocyst-containing ring-shaped bulge (Hu et al., 2012; Gromley et al., 2005). It is, therefore, unclear how intimate the spatial association is in these cells between microtubule overlaps and vesicles (Green et al., 2013). Moss was not shown to have centralspindlin but, MAP65 itself or other midzone-associated proteins, might have a function in Sec6 recruitment to microtubule overlaps. Physical interactions between cytoskeletal regulators and exocyst subunits have been reported in various other systems (van Gisbergen et al., 2018; Gromley et al., 2005; Zuo et al., 2006; Oda et al., 2015). Our MAP65 silencing and Δ*kin4-Ic* experiments clearly showed that the length and presence of microtubule overlaps affected Sec6 localization. Sec6, however, also localized to regions of the phragmoplast midzone that were devoid of MAP65 during later stages of cytokinesis, and Sec6 localized predominantly to the center of long MAP65 regions in Δ*kin4-Ic* cells (Fig. 3). We therefore hypothesize that Sec6 and, possibly, other proteins that are initially on microtubule overlaps are gradually incorporated into another structure to enable vesicle fusion events away from microtubule overlaps. This structure might represent the cell plate assembly matrix (CPAM), which is visible in EM micrographs and from which microtubule overlaps are excluded (Seguí-Simarro et al., 2004). Profound defects in cell plate assembly in cells lacking Kin4 do, however, show that insufficient confinement of initial cell plate depositions around microtubule overlaps is not resolved by successive microtubule-independent processes (de Keijzer et al., 2017).

Our findings provide the first indication that molecules that drive membrane fusion processes are, at least temporarily, associated with microtubule overlaps during plant cytokinesis. The formation of intracellular septa is complex, requiring spatial control over vesicle fusion to produce a new plasma membrane. The involvement of multiple tethering complexes has been reported in several eukaryotes (see Neto and Gould, 2011; Wang et al., 2016; Rybak et al., 2014). Redundancy in the functioning of these complexes might, however, hinder their functional characterization. It will be interesting to learn how the positioning of tethering complexes can fine-tune cell plate formation at the ultrastructural level. Differential localization of TRAPPII and exocyst complexes has been reported during fission yeast cytokinesis, and the two complexes in *Arabidopsis* were alternatingly present at the developing cell plate (Wang et al., 2016; Rybak et al., 2014). The molecular and light microscopic tools available in moss, together with the identification of overlaps as sites of vesicle accumulation, will help to resolve how multiple tethering complexes together shape the cell plate.

Journal of Cell Science (2019) 132, jcs222430. doi:10.1242/jcs.222430

MATERIALS AND METHODS

Plasmids and cloning procedures

All plasmids used throughout this study are listed in Table S2. To construct GFP- and/or mCherry-tagged constructs of Sec6, Sec3a, Sec3b, Sec3c, Sec5a, Sec5b, Sec5d and PpKEULE, regions of ∼1 kb before and after the stop codon of their encoding gene were amplified by PCR using primers listed in Table S1. The PCR fragments were digested with restriction enzymes indicated in Table S1 and ligated into correspondingly digested peGFP-NPTII or pmCherry-LoxP-BsdR vector (de Keijzer et al., 2017).

For RNAi induced by β-estradiol to target the *Sec6* transcript, we used the system published by Nakaoka et al. (2012). A ∼500 bp fragment of the coding sequence of Sec6 (Fig. S5) was amplified by PCR from a cDNA library derived from protonemal tissue and cloned into gateway entry plasmid pENTR-D-TOPO. The fragment was subsequently introduced into silencing vector pGG626 via a Gateway LR reaction.

To generate the expression constructs used for yeast two-hybrid assays, first the coding sequences of Sec6, PpKEULE, and the PpKEULE-C1 domain were PCR-amplified from a *P. patens* cDNA library derived from protonemal tissue. The PCR products were then introduced into the pENTR-D-TOPO vector and subsequently subcloned into destination plasmids pDEST22 and pDEST32 (Invitrogen) via Gateway LR reactions.

For transient small interfering RNA (siRNA) constructs used in RNAi, the region used for induced silencing as described above and regions located at the 5′-untranslated region and the 3′-end of the coding sequence were amplified and cloned into pENTR-D-TOPO (Fig. S6). The fragments were then introduced into the siRNA vector pUGGi (Bezanilla et al., 2005) via a Gateway LR reaction.

P. patens growth conditions and transformation

P. patens tissues were routinely grown on BCDAT plates under continuous light. Plasmids were linearized and introduced into the *P. patens* genome by homologous recombination using PEG-mediated protoplast transformation (Nishiyama et al., 2000). Correct insertion events were characterized by PCR (Fig. S3). RNAi was initiated using β-estradiol treatment and knockdown was verified by quantitative RT-PCR 3 days (Fig. S5). Characteristics of generated moss lines and their use throughout the study are summarized in Table S3. For imaging, protonemal tissue was grown for 5–7 days on BCD medium in glass-bottom dishes (Yamada et al., 2016).

For transient silencing by RNAi, siRNA constructs were transformed into the SNAP-TM-mCherry moss line expressing nuclear targeted GFP-GUS (Van Gisbergen et al., 2018). The nuclear GFP signal was used as a visual marker to identify silenced tissues. Filaments with decreased GFP intensity were selected for analysis (Fig. S6).

Identification of *P. patens* Sec1 homologs

Proteins of the Sec1/Munc18 (SM) family were identified by BLAST using the AtKEULE protein sequence as input against the predicted proteins of *P. patens* genome assembly versions 1.6 and 3.1 (Fig. 5A), and by keyword search in the Phytozome 10.3 browser (www.phytozome.org). Expression in protonema was assessed by verifying the presence of ESTs derived from protonemal tissue and using the *Physcomitrella* eFP browser (Ortiz-Ramírez et al., 2016).

Yeast two-hybrid assay

Yeast two-hybrid assays were performed with a split Gal4 transcription factor system using the His3 gene as reporter (James et al., 1996). For this, pDEST22/32-based constructs (Table S2) were transformed into yeast strain PJ69-4a or PJ69-4α by PEG-mediated transformation. Positive transformants with minimal background reporter activity were selected on synthetic drop-out (SD) medium lacking Leu and His or Trp and His, with different concentrations of 3-amino-1,2,4-triazole (3-AT) to increase histidine-dependent growth stringency. Selected clones were then allowed to mate and resulting diploids were selected on plates lacking Leu and Trp. With surviving cells a yeast two-hybrid assay was then performed on SD medium lacking Leu, Trp and His and in the presence of increasing amounts of 3-AT (1, 2.5 or 15 mM).

Fluorescence microscopy and staining

All live cell imaging was performed on a Roper spinning disk microscope system composed of a Nikon Ti eclipse body, Yokogawa CSU-X1 spinning disc head and Photometrics Evolve 512 camera or Prime 95B camera (Movies 8 and 9). All imaging was conducted with a 100× Plan Apo VC oil immersion objective (NA 1.40), using a 1.2× post-magnification fitted before the camera. The GFP and citrine probes were excited using 491 nm light generated by a Cobolt Calypso50 laser and their emitted light was bandpass filtered at 497–557 nm. For FM4-64 and mCherry 561 nm excitation light generated by a Cobolt Jive50 laser was used in combination with bandpass filtering at 570–620 nm. During image digitization a camera electron multiplication gain of 300 was employed and typical exposures were 800–1000 ms for GFP, citrine and FM4-64, except for Movies 8 and 9, where we used 3000 ms exposure times. For the mCherry probe, exposure times of 1000–2000 ms were used. FM4-64 was dissolved in dH_2O at a final concentration of 10 µM and added to cells at the moment of nuclear envelope breakdown as described (Kosetsu et al., 2013).

Image analysis

FIJI (Schindelin et al., 2012) was used for all image analysis and processing. Figures were prepared in Adobe Illustrator CC 2015. The arrival time of labeled exocyst subunits to the phragmoplast midzone (Fig. 1B) was taken as the time at which structural features with a residence time of more than one time frame first appeared in the generated maximum projections of three image planes. The appearance was abrupt and synchronously over the full length of the midzone. The arrival time of labeled exocyst subunits to a cortical band (Fig. 2C) was defined as the time at which stable cortical patches, visible for more than one time frame, first became visible in the region where the division plane intersected the parental cell wall. These patches were distinctly less dynamic compared to cortical localizations of the exocyst elsewhere in the cell.

Analysis of PpKEULE and membrane accumulation

To quantify the accumulation of cell plate membrane material and PpKEULE upon RNAi to silence *Sec6*, we imaged SCAMP4-mCherry and PpKEULE-GFP throughout cytokinesis at 30 s intervals. Images were taken in the central plane of the dividing cell at three confocal planes spaced 0.5 µm apart. Maximum projections made along the *z*-axis were then used to measure the average intensity of SCAMP4-mCherry and KEULE-GFP using a 5-pixel wide line manually drawn along the division plane for each time point. Simultaneously, the mean level of cytosolic background fluorescence was recorded in an area right next to the cell division site. For each time point, the background fluorescence level was subtracted from the obtained level of fluorescence at the division plane. The expansion rate of the cell plate (Fig. 6D) was calculated as described by de Keijzer et al. (2017).

Gene annotation and expression data

For gene annotation, Cosmoss (www.cosmoss.org/) and the Phytozome 10.3 browser (www.phytozome.org) were used. Gene expression data were obtained from the *Physcomitrella* eFP browser (bar.utoronto.ca/efp_physcomitrella/cgi-bin/efpWeb.cgi).

Acknowledgements

We thank Henk Kieft for technical assistance, Richard Immink and Marco Busscher (WUR-Bioscience, Wageningen, The Netherlands) for assistance with Y2H experiments and Magdalena Bezanilla (Darthmouth College, Hanover, NH) for the kind gift of the pUGGi plasmid.

Competing interests

The authors declare no competing or financial interests.

Author contributions

Conceptualization: J.d.K., M.E.J., T.K.; Methodology: J.d.K., M.E.J., T.K.; Validation: H.T., J.d.K., T.K.; Formal analysis: H.T., J.d.K., E.J.R.O., E.S., M.S.; Investigation: H.T., J.d.K., E.J.R.O., E.S., M.S.; Data curation: J.d.K.; Writing - original draft: J.d.K.; Writing - review & editing: J.d.K., J.E.M.V., M.E.J., T.K.; Visualization: H.T., J.d.K., M.E.J., T.K.; Supervision: J.E.M.V., M.E.J., T.K.; Project administration: J.E.M.V., M.E.J., T.K.; Funding acquisition: J.E.M.V., M.E.J.

Funding
The work has been financially supported by a Human Frontier Science Program (HFSP) grant (grant number: RGP0026/2011 to M.E.J.), by the Earth and Life Sciences Division ALW-VIDI (grant number: 864.13.008 to H.T. and J.E.M.V.) and the Technology Foundation of The Netherlands Organization for Scientific Research (grant number: 831.13.003 to E.J.R.O.).

Supplementary information
Supplementary information available online at
http://jcs.biologists.org/lookup/doi/10.1242/jcs.222430.supplemental

References

Assaad, F. F., Mayer, U., Wanner, G. and Jürgens, G. (1996). The KEULE gene is involved in cytokinesis in *Arabidopsis*. *Mol. Gen. Genet.* **253**, 267-277.
Bezanilla, M., Perroud, P.-F., Pan, A., Klueh, P. and Quatrano, R. S. (2005). An RNAi system in Physcomitrella patens with an internal marker for silencing allows for rapid identification of loss of function phenotypes. *Plant Biol.* **7**, 251-257.
Bloch, D., Pleskot, R., Pejchar, P., Potocký, M., Trpkošová, P., Cwiklik, L., Vukašinović, N., Sternberg, H., Yalovsky, S. and Žárský, V. (2016). Exocyst SEC3 and phosphoinositides define sites of exocytosis in pollen tube initiation and growth. *Plant Physiol.* **172**, 980-1002.
Bodemann, B. O., Orvedahl, A., Cheng, T., Ram, R. R., Ou, Y. -H., Formstecher, E., Maiti, M., Hazelett, C. C., Wauson, E. M., Balakireva, M. et al. (2011). RalB and the exocyst mediate the cellular starvation response by direct activation of autophagosome assembly. *Cell* **144**, 253-267.
Boruc, J. and Van Damme, D. (2015). Endomembrane trafficking overarching cell plate formation. *Curr. Opin. Plant Biol.* **28**, 92-98.
Boyd, C., Hughes, T., Pypaert, M. and Novick, P. (2004). Vesicles carry most exocyst subunits to exocytic sites marked by the remaining two subunits, Sec3p and Exo70p. *J. Cell Biol.* **167**, 889-901.
Buschmann, H. and Zachgo, S. (2016). The evolution of cell division: from streptophyte algae to land plants. *Trends Plant Sci.* **21**, 872-883.
Cvrčková, F., Grunt, M., Bezvoda, R., Hála, M., Kulich, I., Rawat, A. and Zárský, V. (2012). Evolution of the land plant exocyst complexes. *Front. Plant Sci.* **3**, 159.
de Keijzer, J., Kieft, H., Ketelaar, T., Goshima, G. and Janson, M. E. (2017). Shortening of microtubule overlap regions defines membrane delivery sites during plant cytokinesis. *Curr. Biol.* **27**, 514-520.
Doonan, J. H., Cove, D. J. and Lloyd, C. W. (1985). Immunofluorescence microscopy of microtubules in intact cell lineages of the moss, Physcomitrella patens. I. Normal and CIPC-treated tip cells. *J. Cell Sci.* **75**, 131–147.
Drakakaki, G. (2015). Polysaccharide deposition during cytokinesis: challenges and future perspectives. *Plant Sci.* **236**, 177-184.
Drakakaki, G., van de Ven, W., Pan, S., Miao, Y., Wang, J., Keinath, N. F., Weatherly, B., Jiang, L., Schumacher, K., Hicks, G. et al. (2012). Isolation and proteomic analysis of the SYP61 compartment reveal its role in exocytic trafficking in *Arabidopsis*. *Cell Res.* **22**, 413-424.
Dubuke, M. L., Maniatis, S., Shaffer, S. A. and Munson, M. (2015). The exocyst subunit Sec6 interacts with assembled exocytic SNARE complexes. *J. Biol. Chem.* **290**, 28245-28256.
Euteneuer, U. and McIntosh, J. R. (1980). Polarity of midbody and phragmoplast microtubules. *J. Cell Biol.* **87**, 509-515.
Fendrych, M., Synek, L., Pecenková, T., Toupalová, H., Cole, R., Drdová, E., Nebesářová, J., Šedinová, M., Hála, M., Fowler, J. E. et al. (2010). The *Arabidopsis* exocyst complex is involved in cytokinesis and cell plate maturation. *Plant Cell* **22**, 3053-3065.
Fendrych, M., Synek, L., Pečenková, T., Drdová, E. J., Sekereš, J., de Rycke, R., Nowack, M. K. and Žárský, V. (2013). Visualization of the exocyst complex dynamics at the plasma membrane of *Arabidopsis* thaliana. *Mol. Biol. Cell* **24**, 510-520.
Garcia-España, A., Mares, R., Sun, T.-T. and DeSalle, R. (2009). Intron evolution: testing hypotheses of intron evolution using the phylogenomics of tetraspanins. *PLoS ONE* **4**, e4680.
Green, R. A., Mayers, J. R., Wang, S., Lewellyn, L., Desai, A., Audhya, A. and Oegema, K. (2013). The midbody ring scaffolds the abscission machinery in the absence of midbody microtubules. *J. Cell Biol.* **203**, 505-520.
Gromley, A., Yeaman, C., Rosa, J., Redick, S., Chen, C.-T., Mirabelle, S., Guha, M., Sillibourne, J. and Doxsey, S. J. (2005). Centriolin anchoring of exocyst and SNARE complexes at the midbody is required for secretory-vesicle-mediated abscission. *Cell* **123**, 75-87.
Grosshans, B. L., Ortiz, D. and Novick, P. (2006). Rabs and their effectors: achieving specificity in membrane traffic. *Proc. Natl. Acad. Sci. USA* **103**, 11821-11827.
Hála, M., Cole, R., Synek, L., Drdová, E., Pecenková, T., Nordheim, A., Lamkemeyer, T., Madlung, J., Hochholdinger, F., Fowler, J. E. et al. (2008). An exocyst complex functions in plant cell growth in *Arabidopsis* and tobacco. *Plant Cell* **20**, 1330-1345.
Hashizume, K., Cheng, Y.-S., Hutton, J. L., Chiu, C.-H. and Carr, C. M. (2009). Yeast Sec1p functions before and after vesicle docking. *Mol. Biol. Cell* **20**, 4673-4685.
Hazuka, C. D., Foletti, D. L., Hsu, S.-C., Kee, Y., Hopf, F. W. and Scheller, R. H. (1999). The sec6/8 complex is located at neurite outgrowth and axonal synapse-assembly domains. *J. Neurosci.* **19**, 1324-1334.
He, B. and Guo, W. (2009). The exocyst complex in polarized exocytosis. *Curr. Opin. Cell Biol.* **21**, 537-542.
Heider, M. R., Gu, M., Duffy, C. M., Mirza, A. M., Marcotte, L. L., Walls, A. C., Farrall, N., Hakhverdyan, Z., Field, M. C., Rout, M. P. et al. (2016). Subunit connectivity, assembly determinants and architecture of the yeast exocyst complex. *Nat. Struct. Mol. Biol.* **23**, 59-66.
Hiwatashi, Y., Obara, M., Sato, Y., Fujita, T., Murata, T. and Hasebe, M. (2008). Kinesins are indispensable for interdigitation of phragmoplast microtubules in the moss *Physcomitrella patens*. *Plant Cell* **20**, 3094-3106.
Ho, C.-M. K., Hotta, T., Guo, F., Roberson, R. W., Lee, Y.-R. J. and Liu, B. (2011). Interaction of antiparallel microtubules in the phragmoplast is mediated by the microtubule-associated protein MAP65-3 in *Arabidopsis*. *Plant Cell* **23**, 2909-2923.
Hong, W. J. and Lev, S. (2014). Tethering the assembly of SNARE complexes. *Trends Cell Biol.* **24**, 35-43.
Hu, C.-K., Coughlin, M. and Mitchison, T. J. (2012). Midbody assembly and its regulation during cytokinesis. *Mol. Biol. Cell* **23**, 1024-1034.
James, P., Halladay, J. and Craig, E. A. (1996). Genomic libraries and a host strain designed for highly efficient two-hybrid selection in yeast. *Genetics* **144**, 1425-1436.
Javelle, M., Klein-Cosson, C., Vernoud, V., Boltz, V., Maher, C., Timmermans, M., Depège-Fargeix, N. and Rogowsky, P. M. (2011). Genome-wide characterization of the HD-ZIP IV transcription factor family in maize: preferential expression in the epidermis. *Plant Physiol.* **157**, 790-803.
Jürgens, G., Park, M., Richter, S., Touihri, S., Krause, C., El Kasmi, F. and Mayer, U. (2015). Plant cytokinesis: a tale of membrane traffic and fusion. *Biochem. Soc. Trans.* **43**, 73-78.
Karnahl, M., Park, M., Mayer, U., Hiller, U. and Jürgens, G. (2017). ER assembly of SNARE complexes mediating formation of partitioning membrane in *Arabidopsis* cytokinesis. *eLife* **6**, e25327.
Kosetsu, K., de Keijzer, J., Janson, M. E. and Goshima, G. (2013). MICROTUBULE-ASSOCIATED PROTEIN65 is essential for maintenance of phragmoplast bipolarity and formation of the cell plate in *Physcomitrella patens*. *Plant Cell* **25**, 4479-4492.
Kosetsu, K., Murata, T., Yamada, M., Nishina, M., Boruc, J., Hasebe, M., Van Damme, D. and Goshima, G. (2017). Cytoplasmic MTOCs control spindle orientation for asymmetric cell division in plants. *Proc. Natl. Acad. Sci. USA* **114**, 8847-8854.
Koumandou, V. L., Dacks, J. B., Coulson, R. M. R. and Field, M. C. (2007). Control systems for membrane fusion in the ancestral eukaryote; evolution of tethering complexes and SM proteins. *BMC Evol. Biol.* **7**, 29.
Kulich, I., Pečenková, T., Sekereš, J., Smetana, O., Fendrych, M., Foissner, I., Höftberger, M. and Zárský, V. (2013). *Arabidopsis* exocyst subcomplex containing subunit EXO70B1 is involved in autophagy-related transport to the vacuole. *Traffic* **14**, 1155-1165.
Lee, Y. R., Giang, H. M. and Liu, B. (2001). A novel plant kinesin-related protein specifically associates with the phragmoplast organelles. *Plant Cell* **13**, 2427-2439.
Lipka, E., Gadeyne, A., Stöckle, D., Zimmermann, S., De Jaeger, G., Ehrhardt, D. W., Kirik, V., Van Damme, D. and Müller, S. (2014). The phragmoplast-orienting kinesin-12 class proteins translate the positional information of the preprophase band to establish the cortical division zone in Arabidopsis thaliana. *Plant Cell* **26**, 2617-2632.
Liu, Q., Liu, F., Yu, K. L., Tas, R., Grigoriev, I., Remmelzwaal, S., Serra-Marques, A., Kapitein, L. C., Heck, A. J. R. and Akhmanova, A. (2016). MICAL3 flavoprotein monooxygenase forms a complex with centralspindlin and regulates cytokinesis. *J. Biol. Chem.* **291**, 20617-20629.
Luo, G., Zhang, J. and Guo, W. (2014). The role of Sec3p in secretory vesicle targeting and exocyst complex assembly. *Mol. Biol. Cell* **25**, 3813-3822.
McMichael, C. M. and Bednarek, S. Y. (2013). Cytoskeletal and membrane dynamics during higher plant cytokinesis. *New Phytol.* **197**, 1039-1057.
Miki, T., Naito, H., Nishina, M. and Goshima, G. (2014). Endogenous localizome identifies 43 mitotic kinesins in a plant cell. *Proc. Natl. Acad. Sci. USA* **111**, 1053-1061.
Morgera, F., Sallah, M. R., Dubuke, M. L., Gandhi, P., Brewer, D. N., Carr, C. M. and Munson, M. (2012). Regulation of exocytosis by the exocyst subunit Sec6 and the SM protein Sec1. *Mol. Biol. Cell* **23**, 337-346.
Müller, S. and Jürgens, G. (2015). Plant cytokinesis - no ring, no constriction but centrifugal construction of the partitioning membrane. *Semin. Cell Dev. Biol.* **53**, 10-18.
Müller, S., Wright, A. J. and Smith, L. G. (2009). Division plane control in plants: new players in the band. *Trends Cell Biol.* **19**, 180-188.
Nakaoka, Y., Miki, T., Fujioka, R., Uehara, R., Tomioka, A., Obuse, C., Kubo, M., Hiwatashi, Y. and Goshima, G. (2012). An inducible RNA interference system in *Physcomitrella patens* reveals a dominant role of augmin in phragmoplast microtubule generation. *Plant Cell* **24**, 1478-1493.

Neto, H. and Gould, G. W. (2011). The regulation of abscission by multi-protein complexes. *J. Cell Sci.* **124**, 3199-3207.
Nishiyama, T., Hiwatashi, Y., Sakakibara, I., Kato, M. and Hasebe, M. (2000). Tagged mutagenesis and gene-trap in the moss, *Physcomitrella patens* by shuttle mutagenesis. *DNA Res.* **7**, 9-17.
Oda, Y., Iida, Y., Nagashima, Y., Sugiyama, Y. and Fukuda, H. (2015). Novel coiled-coil proteins regulate exocyst association with cortical microtubules in xylem cells via the conserved oligomeric golgi-complex 2 protein. *Plant Cell Physiol.* **56**, 277-286.
Ortiz-Ramírez, C., Hernandez-Coronado, M., Thamm, A., Catarino, B., Wang, M., Dolan, L., Feijó, J. A. and Becker, J. D. (2016). A transcriptome atlas of *Physcomitrella patens* provides insights into the evolution and development of land plants. *Mol. Plant* **9**, 205-220.
Otegui, M. and Staehelin, L. A. (2000). Syncytial-type cell plates: a novel kind of cell plate involved in endosperm cellularization of Arabidopsis. *Plant Cell* **12**, 933-947.
Otegui, M. S., Mastronarde, D. N., Kang, B. H., Bednarek, S. Y. and Staehelin, L. A. (2001). Three-dimensional analysis of syncytial-type cell plates during endosperm cellularization visualized by high resolution electron tomography. *Plant Cell* **13**, 2033-2051.
Park, M., Touihri, S., Müller, I., Mayer, U. and Jürgens, G. (2012). Sec1/Munc18 protein stabilizes fusion-competent syntaxin for membrane fusion in *Arabidopsis* cytokinesis. *Dev. Cell* **22**, 989-1000.
Paumet, F., Rahimian, V. and Rothman, J. E. (2004). The specificity of SNARE-dependent fusion is encoded in the SNARE motif. *Proc. Natl. Acad. Sci. USA* **101**, 3376-3380.
Picco, A., Irastorza-Azcarate, I., Specht, T., Böke, D., Pazos, I., Rivier-Cordey, A.-S., Devos, D. P., Kaksonen, M. and Gallego, O. (2017). The in vivo architecture of the exocyst provides structural basis for exocytosis. *Cell* **168**, 400-412.e18.
Qi, X., Kaneda, M., Chen, J., Geitmann, A. and Zheng, H. (2011). A specific role for *Arabidopsis* TRAPPII in post-Golgi trafficking that is crucial for cytokinesis and cell polarity. *Plant J.* **68**, 234-248.
Rawat, A., Brejšková, L., Hála, M., Cvrčková, F. and Žárský, V. (2017). The *Physcomitrella patens* exocyst subunit EXO70.3d has distinct roles in growth and development, and is essential for completion of the moss life cycle. *New Phytol.* **216**, 438-454.
Rensing, S. A., Fritzowsky, D., Lang, D. and Reski, R. (2005). Protein encoding genes in an ancient plant: analysis of codon usage, retained genes and splice sites in a moss, *Physcomitrella patens*. *BMC Genomics* **6**, 43.
Richter, S., Kientz, M., Brumm, S., Nielsen, M. E., Park, M., Gavidia, R., Krause, C., Voss, U., Beckmann, H., Mayer, U. et al. (2014). Delivery of endocytosed proteins to the cell-division plane requires change of pathway from recycling to secretion. *eLife* **3**, e02131.
Rogozin, I. B., Wolf, Y. I., Sorokin, A. V., Mirkin, B. G. and Koonin, E. V. (2003). Remarkable interkingdom conservation of intron positions and massive, lineage-specific intron loss and gain in eukaryotic evolution. *Curr. Biol.* **13**, 1512-1517.
Rybak, K., Steiner, A., Synek, L., Klaeger, S., Kulich, I., Facher, E., Wanner, G., Kuster, B., Žárský, V., Persson, S. et al. (2014). Plant cytokinesis is orchestrated by the sequential action of the TRAPPII and exocyst tethering complexes. *Dev. Cell* **29**, 607-620.
Schaefer, E., Belcram, K., Uyttewaal, M., Duroc, Y., Goussot, M., Legland, D., Laruelle, E., de Tauzia-Moreau, M.-L., Pastuglia, M. and Bouchez, D. (2017). The preprophase band of microtubules controls the robustness of division orientation in plants. *Science* **356**, 186-189.
Schindelin, J., Arganda-Carreras, I., Frise, E., Kaynig, V., Longair, M., Pietzsch, T., Preibisch, S., Rueden, C., Saalfeld, S., Schmid, B. et al. (2012). Fiji: an open-source platform for biological-image analysis. *Nat. Methods* **9**, 676-682.
Schmiedel, G., Reiss, H.-D. and Schnepf, E. (1981). Associations between membranes and microtubules during mitosis and cytokinesis in caulonema tip cells of the moss Funaria hygrometrica. *Protoplasma* **108**, 173-190.
Seguí-Simarro, J. M., Austin, J. R., II, White, E. A. and Staehelin, L. A. (2004). Electron tomographic analysis of somatic cell plate formation in meristematic cells of *Arabidopsis* preserved by high-pressure freezing. *Plant Cell* **16**, 836-856.
Sivaram, M. V. S., Saporita, J. A., Furgason, M. L. M., Boettcher, A. J. and Munson, M. (2005). Dimerization of the exocyst protein Sec6p and its interaction with the t-SNARE Sec9p. *Biochemistry* **44**, 6302-6311.
Sivaram, M. V. S., Furgason, M. L. M., Brewer, D. N. and Munson, M. (2006). The structure of the exocyst subunit Sec6p defines a conserved architecture with diverse roles. *Nat. Struct. Mol. Biol.* **13**, 555-556.
Smertenko, A., Assaad, F., Baluška, F., Bezanilla, M., Buschmann, H., Drakakaki, G., Hauser, M.-T., Janson, M., Mineyuki, Y., Moore, I. et al. (2017). Plant cytokinesis: terminology for structures and processes. *Trends Cell Biol.* **27**, 885-894.
Söllner, T., Whiteheart, S. W., Brunner, M., Erdjument-Bromage, H., Geromanos, S., Tempst, P. and Rothman, J. E. (1993). SNAP receptors implicated in vesicle targeting and fusion. *Nature* **362**, 318-324.
Spinner, L., Pastuglia, M., Belcram, K., Pegoraro, M., Goussot, M., Bouchez, D. and Schaefer, D. G. (2010). The function of TONNEAU1 in moss reveals ancient mechanisms of division plane specification and cell elongation in land plants. *Development* **137**, 2733-2742.
Steiner, A., Müller, L., Rybak, K., Vodermaier, V., Facher, E., Thellmann, M., Ravikumar, R., Wanner, G., Hauser, M.-T. and Assaad, F. F. (2016). The membrane-associated Sec1/Munc18 KEULE is required for phragmoplast microtubule reorganization during cytokinesis in *Arabidopsis*. *Mol. Plant* **9**, 528-540.
Stenmark, H. (2009). Rab GTPases as coordinators of vesicle traffic. *Nat. Rev. Mol. Cell Biol.* **10**, 513-525.
Stöckle, D., Herrmann, A., Lipka, E., Lauster, T., Gavidia, R., Zimmermann, S. and Müller, S. (2016). Putative RopGAPs impact division plane selection and interact with kinesin-12 POK1. *Nat. Plants* **2**, 16120.
Südhof, T. C. and Rothman, J. E. (2009). Membrane fusion: grappling with SNARE and SM proteins. *Science* **323**, 474-477.
Synek, L., Vukašinović, N., Kulich,I., Hála, M., Aldorfová, K., Fendrych, M. and Žárský, V. (2017). EXO70C2 is a key regulatory factor for optimal tip growth of pollen. *Plant Physiol.* **174**, 223-240.
TerBush, D. R. and Novick, P. (1995). Sec6, Sec8, and Sec15 are components of a multisubunit complex which localizes to small bud tips in Saccharomyces cerevisiae. *J. Cell Biol* **130**, 299-312.
Thellmann, M., Rybak, K., Thiele, K., Wanner, G. and Assaad, F. F. (2010). Tethering factors required for cytokinesis in *Arabidopsis*. *Plant Physiol.* **154**, 720-732.
Van Damme, D. (2009). Division plane determination during plant somatic cytokinesis. *Curr. Opin. Plant Biol.* **12**, 745-751.
van Gisbergen, P. A. C., Wu, S.-Z., Chang, M., Pattavina, K. A., Bartlett, M. E. and Bezanilla, M. (2018). An ancient Sec10–formin fusion provides insights into actin-mediated regulation of exocytosis. *J. Cell Biol.* **217**, 945-957.
Vukašinović, N. and Žárský, V. (2016). Tethering complexes in the *Arabidopsis* endomembrane system. *Front. Cell Dev. Biol.* **4**, 46.
Wang, N., Lee, I.-J., Rask, G. and Wu, J.-Q. (2016). Roles of the TRAPP-II complex and the exocyst in membrane deposition during fission yeast cytokinesis. *PLoS Biol.* **14**, e1002437.
Wickner, W. and Schekman, R. (2008). Membrane fusion. *Nat. Struct. Mol. Biol.* **15**, 658-664.
Wu, S.-Z., Ritchie, J. A., Pan, A.-H., Quatrano, R. S. and Bezanilla, M. (2011). Myosin VIII regulates protonemal patterning and developmental timing in the moss *Physcomitrella patens*. *Mol. Plant* **4**, 909-921.
Wu, J., Tan, X., Wu, C., Cao, K., Li, Y. and Bao, Y. (2013). Regulation of cytokinesis by exocyst subunit SEC6 and KEULE in *Arabidopsis* thaliana. *Mol. Plant* **6**, 1863-1876.
Wu, S. Z. and Bezanilla, M. (2014). Myosin VIII associates with microtubule ends and together with actin plays a role in guiding plant cell division. *eLife* **3**, e03498.
Yamada, M., Miki, T. and Goshima, G. (2016). Imaging mitosis in the moss *Physcomitrella patens*. In *Methods in Molecular Biology (Clifton, N.J.)* (ed. P. Chang and R. Ohi), pp. 263-282. New York, NY, United States: Springer New York.
Yu, I.-M. and Hughson, F. M. (2010). Tethering factors as organizers of intracellular vesicular traffic. *Annu. Rev. Cell Dev. Biol.* **26**, 137-156.
Zhang, Y., Immink, R., Liu, C.-M., Emons, A. M. and Ketelaar, T. (2013). The *Arabidopsis* exocyst subunit SEC3A is essential for embryo development and accumulates in transient puncta at the plasma membrane. *New Phytol.* **199**, 74-88.
Zuo, X., Zhang, J., Zhang, Y., Hsu, S.-C., Zhou, D. and Guo, W. (2006). Exo70 interacts with the Arp2/3 complex and regulates cell migration. *Nat. Cell Biol.* **8**, 1383-1388.